Zheng, J. & Hryciw, R. D. (2015). *Géotechnique* **65**, No. 6, 494–506 [http://dx.doi.org/10.1680/geot.14.P.192]

Traditional soil particle sphericity, roundness and surface roughness by computational geometry

J. ZHENG* and R. D. HRYCIW*

Definitions of soil particle sphericity, roundness and roughness have existed since at least the 1930s. In the 1950s, charts of typical sphericity and roundness values were developed to alleviate tedious manual determination. They allowed users to classify particles by visual comparison to typical particles possessing ranges of sphericity and roundness. The original definitions and somewhat subjective chart methods are still widely used today. This paper describes robust numerical methods based on computational geometry to determine precisely the traditional values from two-dimensional images of particles. Statistical methods including locally weighted regression and *K*-fold cross-validation were used to discretise a mean particle surface and thereby quantify and remove roughness. The paper details the algorithms for identifying particle corners and fitting circles to them for computation of roundness. Conclusions are also drawn regarding the most appropriate definition for particle sphericity from among five that are commonly cited. Finally, recommendations are made for the minimum image resolutions and particle perimeter discretisation necessary to obtain accurate results.

KEYWORDS: geology; gravels; particle-scale behaviour; sands; soil classification

INTRODUCTION

Soil particle shape is defined by international standards (ISO, 2008) as 'the envelope formed by all the points on the surface of the particle'. Using two-dimensional projections, it may be characterised at three observation levels as shown in Fig. 1. From largest to smallest scale, particles are described by their: form, roundness and surface texture (Barrett, 1980; Mitchell & Soga, 2005; ISO, 2008). For soil particles, 'sphericity' is commonly used for describing form, while 'roughness' is often used for surface texture. Therefore, in this paper, the authors will use the common geotechnical terms: sphericity, roundness and roughness. The three are considered to be independent descriptors of particle shape because each can vary with no change in the other two (Wadell, 1932; Barrett, 1980; Cho *et al.*, 2006). Although it is well established that these intrinsic particle characteristics affect various soil macro-scale properties, they are often ignored in practice because of the effort required to determine them.

As numerical modelling of soils at the discrete level matures, it is also becoming incumbent to utilise real particle geometries in the models. This presents two challenges: how to efficiently extract particle shapes (sphericity, roundness and roughness) of a statistically significant number of particles and how to reproduce those complex particle shapes in discrete-element methods (DEMs). Significant advances have been made to generate the complex particle shapes in DEM. For example, a popular technique is to cluster discs or spheres to create complex shapes as in the works of Katagiri *et al.* (2010) and Ferellec & McDowell (2010). More sophisticated methods, which could create realistic packing of particles with complex shapes, include a Voronoi-based spheropolyhedra algorithm introduced by Galindo-Torres & Pedroso (2010) and Galindo-Torres & Muñoz (2010) and a Fourier–Voronoi-based algorithm presented by Mollon & Zhao (2012a, 2012b, 2014). However, the problem of how to effectively determine particle sphericity, roundness and roughness of real soils has remained a challenge. Therefore, this paper describes an automated, non-subjective method to determine all three descriptors using computational geometry. The presented algorithms could be used by practitioners and researchers to determine the shape parameters quickly and could also eventually assist micro-mechanicians in generation of more realistic DEM models.

Sphericity

The first description of sphericity for 'objects of sedimentological importance' is generally attributed to Wadell (1933). He defined 'degree of true sphericity' as 'the ratio of the surface area of a sphere of the same volume as the particle to the actual surface area of the particle'. Recognising the difficulty of measuring three-dimensional surface areas of soil particles, Wadell also offered a practical definition based on the projected area of a particle; he defined 'degree of sphericity' as the diameter of a circle having an area equal to the largest projected area to the diameter of the smallest circle that will circumscribe the grain projection. Over the years, other definitions of sphericity have been proposed (Krumbein & Sloss, 1951; Santamarina & Cho, 2004; Mitchell & Soga, 2005; Altuhafi *et al.*, 2013). As such, some confusion exists as to the practical differences between the definitions and there is uncertainty as to which is most

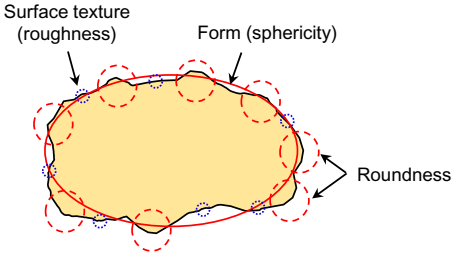

Fig. 1. Particle shape characterisation at different scales (after Barrett, 1980; Mitchell & Soga, 2005; ISO, 2008)

Manuscript received 26 September 2014; revised manuscript accepted 10 February 2015.
Discussion on this paper closes on 1 November 2015, for further details see p. ii.
* Department of Civil and Environmental Engineering, University of Michigan, Ann Arbor, MI, USA.

useful and effective in describing particle form. Therefore, the first objective of this paper is to compare the various definitions of sphericity, describe the methods used to quantify them and compare their usefulness and effectiveness relative to each other.

Roundness

Roundness quantifies the sharpness of particle corners. It was first distinguished from sphericity by Wadell (1932, 1933, 1935). Using two-dimensional projections of particles, Wadell defined roundness as the ratio of the average radius of curvature of the corners of a particle to the radius of the maximum inscribed circle. This definition of roundness is still widely used today (Santamarina & Cho, 2004; Mitchell & Soga, 2005; Cho *et al*., 2006; Bareither *et al.*, 2008; Chapuis, 2012; Cabalar *et al.*, 2013; Shin & Santamarina, 2013). The original procedure for determination of Wadell's roundness requires considerable manual effort. Each corner on a particle's outline is compared to a series of transparent templates to find the maximum sized circle that will fit inside the corner. Despite being cumbersome and subjective, the procedure is still used today (Moroto & Ishii, 1990; Rouse *et al.*, 2008; Oh *et al.*, 2014).

Chart methods for roundness and sphericity

In the 1950s, charts consisting of a set of reference particle silhouettes were prepared to facilitate rapid estimation of Wadell's particle roundness through visual comparisons to particles viewed under a microscope. Three such charts were developed by Krumbein (1941), Krumbein & Sloss (1951) and Powers (1953). The Krumbein and Sloss chart also provided an estimate of sphericity but, as indicated earlier, some confusion exists as to which definition of sphericity was used. Obviously, the charts are even more subjective than Wadell's original template method. Nevertheless, they are used in many disciplines including geotechnical engineering, soil science, agriculture, powder engineering, pavement engineering and geology. Studies have compared the effects of soil particle shape and roundness as obtained from the charts on the macroscale properties and mechanical behavior of soil (Youd, 1973; Edil *et al.*, 1975; Frossard, 1979; Sladen *et al.*, 1985; Santamarina & Cho, 2004; Bareither *et al.*, 2008; Chapuis, 2012; Cabalar *et al.*, 2013; Shin & Santamarina, 2013; Kandasami & Murthy, 2014). In geomorphology, Eisma (1965) studied the influence of roundness of beach and dune sands on eolian sorting. Sagga (1993) assessed the roundness of sand grains in longitudinal dunes in Saudi Arabia. Mehring & McBride (2007) used the charts in studies on the origin of beach sands. Vepraskas & Cassel (1987) studied the influence of sphericity and roundness of coastal plain sands on soils' resistance to cone penetration, to bulk density, and on the angle of repose of dense sands. In all of the above-mentioned research, roundness was determined using the charts. The charts have also been used for comparison to other roundness descriptors such as proposed by Masad *et al.* (2007) and Sukumaran & Ashmawy (2001).

Advances in optical image gathering have led to rapid digitisation of soil particle projections and created a potential to automate Wadell's procedure. It has nevertheless been a mathematically challenging problem and thus, researchers have proposed alternative definitions of roundness which could be more easily computerised. Such alternative definitions have included: Fourier analysis (Bowman *et al.*, 2001; Wettimuny & Penumadu, 2004; Wang *et al.*, 2005), angularity index (Sukumaran & Ashmawy, 2001; Tutumluer & Pan, 2008), and a fractal technique (Arasan *et al.*, 2011). A comprehensive review of these newer methods was provided by Masad *et al.* (2007). However, the alternative definitions of roundness have not yet prevailed over Wadell's, owing to the latter's longer history and numerous useful correlations to mechanical properties based on it. In light of its continuing popularity and wide usage, the second objective of this paper is to develop an algorithm, based on computational geometry and statistics, to automate a rigorous and non-subjective determination of roundness according to Wadell's definition.

Surface roughness

At the smallest observation scale there is surface roughness. The direct measurement of roughness is difficult because its value is scale dependent (Santamarina & Cho, 2004). As its third objective, this paper presents an approach for evaluating the surface roughness of soil particles based on two statistical methods: locally weighted regression smoothing (LOESS) and *K*-fold cross-validation. The mean surface obtained using LOESS and *K*-fold cross-validation will be used to eliminate the effect of surface roughness in the assessment of particle roundness.

By necessity, the paper is organised in a different order than presented above. First, five sphericity definitions are introduced. Next, a roughness assessment method is presented. Removal of roughness is prerequisite to the determination of the mean particle surface, which in turn is used in the new algorithm for computing Wadell's roundness. Finally, the computer-based results are compared to roundness values obtained manually by Wadell (1935) and to particles shown in the Krumbein & Sloss (1951) chart, with the expectation that high correlations will eliminate the need for manual procedures and chart-based approximations.

SPHERICITY BY COMPUTATIONAL GEOMETRY

As previously mentioned, particle sphericity has been defined in various ways. The five most commonly used definitions as reviewed by Mitchell & Soga (2005) and Rodriguez *et al.* (2012) are

area sphericity

$$S_A = \frac{A_s}{A_{cir}} \tag{1}$$

diameter sphericity

$$S_D = \frac{D_c}{D_{cir}} \tag{2}$$

circle ratio sphericity

$$S_C = \frac{D_{ins}}{D_{cir}} \tag{3}$$

perimeter sphericity

$$S_P = \frac{P_c}{P_s} \tag{4}$$

width to length ratio sphericity

$$S_{WL} = \frac{d_2}{d_1} \tag{5}$$

where A_s is the projected area of a soil particle; A_{cir} is the area of the minimum circumscribing circle; D_c is the diameter of a circle having the same projected area as the particle; D_{cir} is the diameter of the minimum circumscribing circle; D_{ins} is the diameter of the largest inscribing circle; P_c is the perimeter of a circle having the same projected area as the particle; P_s is the perimeter of the particle; and d_1 and d_2

are the length and width of a particle.

Volume-based sphericity definitions, such as proposed by Wadell (1933), also exist but they are not used in this paper since the soil particles are being characterised strictly from two-dimensional projections.

Area sphericity was first proposed by Tickell (1931). Diameter sphericity is, according to Wadell (1933), the original 'degree of true sphericity'. The area sphericity is the square of diameter sphericity. Riley (1941) defined $\sqrt{D_{\text{ins}}/D_{\text{cir}}}$ as sphericity, which later evolved into S_C by equation (3) in papers by Santamarina & Cho (2004) and Cho *et al.* (2006). Similarly, Cox (1927) defined sphericity by $(P_c/P_s)^2$ which evolved into S_P by equation (4) in the works of Kuo & Freeman (2000) and Altuhafi *et al.* (2013). The S_P is identical to 'circularity' in ISO (2008). For historical accuracy, neither Tickell (1931) nor Cox (1927) actually used the term 'sphericity'; in the pre-Wadell era, they used the term 'roundness' for today's 'sphericity'. Krumbein & Sloss (1951) hinted that 'sphericity could be related to the proportion between length and breadth of the particles'. The authors believe that Krumbein and Sloss must have had equation (5) in mind. The reciprocal of S_{WL} is commonly referred to as the 'elongation ratio'.

The area and perimeter of a soil particle can be easily determined in Matlab, the image processing package from MathWorks (2014). However, the minimum circumscribing circle, the maximum inscribed circle, and the particle length and width must be determined through additional 'computational geometry' as follows.

The outline of a soil particle can be discretised as shown in Fig. 2(a). The process of finding the minimum circumscribing circle is shown in Figs 2(b), 2(c) and 2(d). First, the minimum number of outer points which when connected will bound all of the others is found. This is shown by the eight points in Fig. 2(b). The two points which are farthest from each other (no. 1 and no. 5) define the diameter of a trial circle as shown in Fig. 2(c). If all of the other points are within this circle, then this is the minimum circumscribing circle. If not, the point which lies furthest outside of the circle (no. 7) is added to the first two points and a new circle is fitted to the three points (no. 1, no. 5 and no. 7). If all the other points are within this circle, this is a minimum circumscribing circle. If not, the point which lies furthest outside of the circle is added and a new circle is found using any two or three of the four points. The procedure is repeated until no points lie outside the circle. This yields the minimum circumscribing circle for the original set of points, as shown in Fig. 2(d).

The measurements of length and width of soil particles in this paper mimic the procedure of ASTM D4791-10 (ASTM, 2010) and ASTM D2488-09a (ASTM, 2009). Conceptually, the soil particle is circumscribed by a rectangular bounding box. Trial boxes with orientations ranging over 180° are fitted to circumscribe the eight outer points, as shown in Figs 2(e)–2(h). The box that displays the largest single dimension (Fig. 2(f)) defines both the length and width of the particle.

The maximum inscribed circle may be determined using a Euclidean distance map. For each pixel inside the soil particle in Fig. 3(a), the distance to the nearest boundary pixel is computed, resulting in the Euclidean distance map as shown in Fig. 3(b). The largest distance value and its location identify the radius, R_i, and the centre of the maximum inscribed circle, C_i, as shown in Fig. 3(b). The results (in pixel units) are summarised in Fig. 3(c).

SURFACE ROUGHNESS BY COMPUTATIONAL GEOMETRY

Locally weighted regression smoothing

All surfaces are rough even down to the atomic scale. In general, instruments with different resolutions and scan lengths will yield different roughness values for the same surface (Majumdar & Bhushan, 1990). Given measurements at a specific scale, the deviations of a surface from its mean plane are commonly used to characterise the roughness at the given scale. However, because of highly irregular soil particle surfaces, there is generally no functional form to describe the mean surface. This problem can be addressed by non-parametric fitting techniques. Such techniques fit a smooth curve to the measured points without any prior specification of a functional relationship between the points. One of the most popular non-parametric smoothers is 'locally weighted scatter plot smoothing' (LOESS), which was proposed by Cleveland & Devlin (1988). An example of the LOESS procedure is shown in Fig. 4. In Fig. 4(a), a mean surface was assumed to be defined by the arbitrary function $y = 2 - \cos(0{\cdot}6x) - \sin(0{\cdot}6x) - \cos(1{\cdot}2x) - \sin(1{\cdot}2x)$. Over the X-range shown in Fig. 4(a), the function could be representing a corner of a sub-angular soil particle. The authors added Gaussian noise around the mean surface to generate a 'rough' surface. The 'roughness' could be actual particle

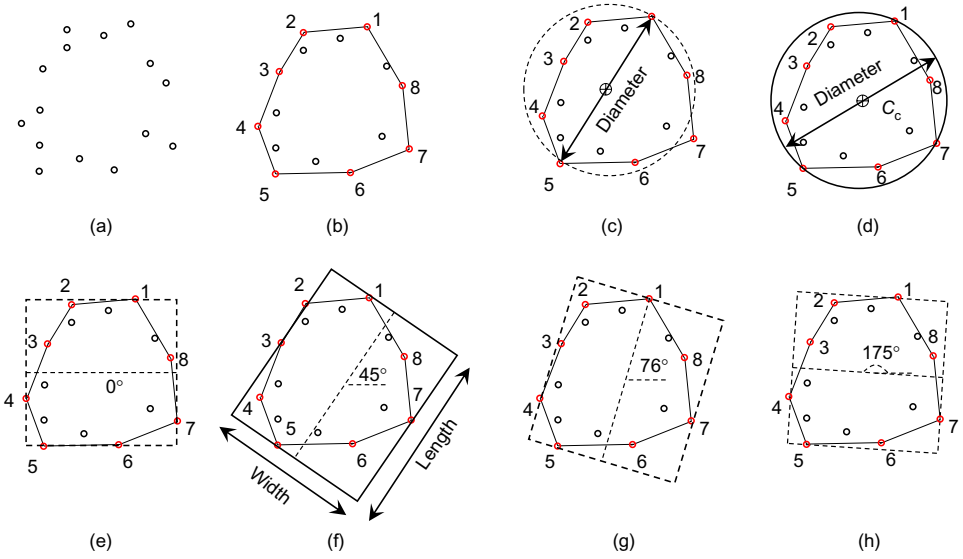

Fig. 2. Finding the minimum circumscribing circle, length and width of a particle

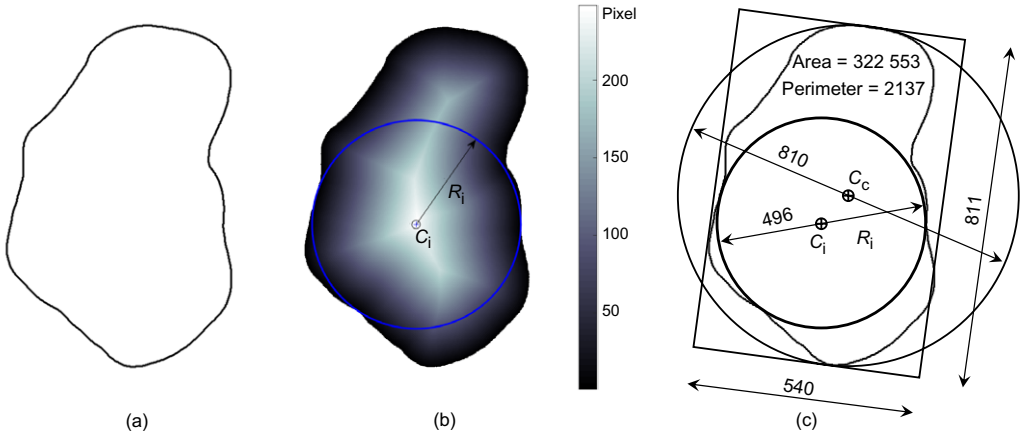

Fig. 3. Finding the maximum inscribed circle of a soil particle: (a) particle outline; (b) Euclidean distance map; (c) result in pixel units

roughness or digital rounding to pixels or simply electrical noise in the measurement system (e.g. camera, scanner or profilometer). In any case, the open circles in Fig. 4(a) represent an instrument's measurements of this surface. The measurement could be optical or physical and they could be at any scale depending on the instrument used. The measurement interval depends on the resolution of the instrument at this scale. The actual mean surface is now presumed to be unknown. The goal of LOESS is to predict the mean surface from the rough measurements.

LOESS replaces each data point with the smoothed value determined by a locally weighted regression. Fig. 4(b) shows how a smoothed value is found for a point x_i located between $X=2{\cdot}5$ and $X=3{\cdot}0$. The point x_i and its nearest neighbouring points over a span distance α are used in the process. The span α is the ratio of the number of data points used for fitting to the total number of data points. Therefore, α is a value between 0 and 1·0. In this example, there are, in total, 200 measurement points in a range between $X=2{\cdot}0$ and $X=6{\cdot}0$. If $\alpha=0{\cdot}045$ then nine points would be used for each smoothing. For each point in the span, a weight is applied based on its distance to the centre point x_i. For example, the weight for the kth point in Fig. 4(b) could be

$$w_k = \exp\left[-\frac{(x_i - x_k)^2}{2\alpha^2}\right] \tag{6}$$

The function is plotted in Fig. 4(b). It shows that points closer to x_i have larger weights and therefore more influence on the fitting.

After applying weights to the data points in the span, a second-degree polynomial is fitted to the points using least-square regression. The smoothed value at point x_i will be given by the weighted regression as shown in Fig. 4(b). This smoothing process progresses from data point to data point to obtain the smoothed value of each point. Clearly, the computed smoothed values will be affected by the specified α. Fig. 4(c) shows three LOESS curves that were fitted to the same measured data with α having been varied from 0·02 to 0·90. It is evident that small α values could not filter out the roughness, while large α values yield curves that fail to follow the local curvilinearity. The selection of an appropriate α must compromise between the 'over-fitting' and 'under-fitting' to produce a LOESS curve which is as close as possible to the mean surface. A strategy for finding the proper α follows.

K-*fold cross-validation*

The optimal α value can be determined by cross-validation techniques (Efron & Tibshirani, 1993). Cross-validation is essentially a trial-and-error approach. A total of say N different α values are tested one by one. The α producing the minimum fitting error is the optimum. A popular cross-validation technique is called K-fold cross-validation. The procedure is represented diagrammatically in Fig. 5. All of the measured data points defining a particle's outline are randomly partitioned into K roughly equal-sized sets. As shown by the rows in Fig. 5, each of the sets will, in turn, be used as a validation set while the remaining sets are training sets. For

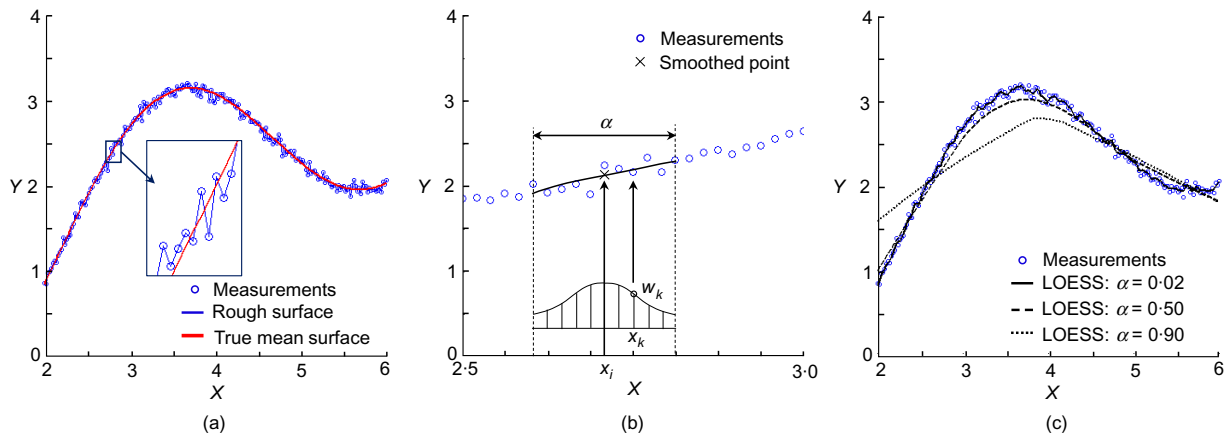

Fig. 4. The LOESS procedure and results by various α values

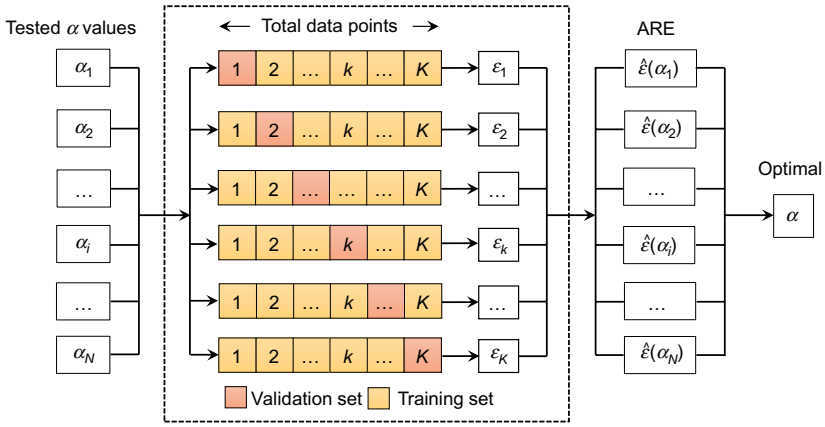

Fig. 5. Procedure for *K*-fold cross-validation

example, in the kth row, the kth set is the validation set, whereas the others are training sets. The data from all of the training sets are fitted with a LOESS curve, which is defined by the α value being tested. The validation set is then used to calculate a residual error for this LOESS curve. For the ith α value and the kth row it is $\varepsilon_k(\alpha_i)$. This process is repeated K times for $k=1, 2, \ldots, K$. The error for each tested span α_i is then calculated as the average residual error (ARE) of $\varepsilon_k(\alpha_i)$

$$\hat{\varepsilon}(\alpha_i) = \frac{1}{K}\sum_{k=1}^{K}\varepsilon_k(\alpha_i) \tag{7}$$

The α with the minimum $\hat{\varepsilon}$ is the optimal span value. A series of K values was tried in this study. The results showed that $K=10$ is adequate for soil particle roughness analysis.

Back to the example given in Fig. 4, in order to find the optimal α, a series of values from 0·01 to 0·99 with increments of 0·0098 (a total of 100 α values) were evaluated using ten-fold cross-validation. In total, 200 data points were randomly divided into ten sets. Each set contained 20 points. For every tested span α_i ($i=1, 2, \ldots, 100$), a training set containing 180 data points was fitted by a LOESS curve, as shown in Fig. 6(a). The validation set, consisting of the remaining 20 points, was then used to compute the residual error. This process was repeated ten times for each α_i to obtain its average residual error $\hat{\varepsilon}(\alpha_i)$. The optimal α was found to be 0·3367 based on the minimum ARE. Using $\alpha=0{\cdot}3367$, the LOESS curve is fitted using all of the measurements. The result is shown in Fig. 6(b). The LOESS curve overlaps the true mean surface almost perfectly. The largest discrepancy between the two curves is 0·001. In summary, provided the roughness measurements, LOESS combined with K-fold cross-validation effectively predicts the mean surface.

Having established the smoothed surface, a commonly used root-mean-squared roughness can be computed

$$\text{Roughness} = \sqrt{\frac{1}{N}\sum_{i=1}^{N}(y_i - y_{i-\text{LOESS}})^2} \tag{8}$$

where y_i is ith measurement; $y_{i\text{-LOESS}}$ is the smoothed ith measurement on the LOESS curve; and N is the total number of measurements. It should be noted that roughness values computed from equation (8) would vary with different scales. Therefore, equation (8) must be used at the scale relevant to the problem being addressed.

To assess the roughness of a soil particle such as the one shown in Fig. 7(a), the points on the particle outline are traced out using polar coordinates, as shown in Fig. 7(b). This particle image has a resolution of 40 pixel/mm. The (θ, ρ) coordinates of a total of 1980 points are plotted in Figs 7(b) and 7(c). Using LOESS and ten-fold cross-validation, the optimal α was found to be 0·015. The predicted mean surface of this soil particle is shown as the dashed line in Fig. 7(c). The computed roughness using equation (7) is 0·1 mm.

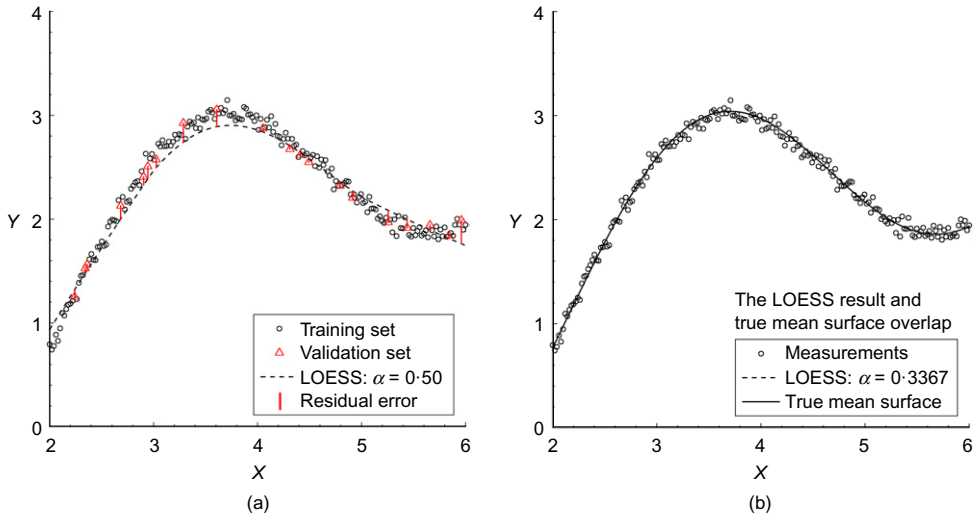

Fig. 6. A ten-fold cross-validation result

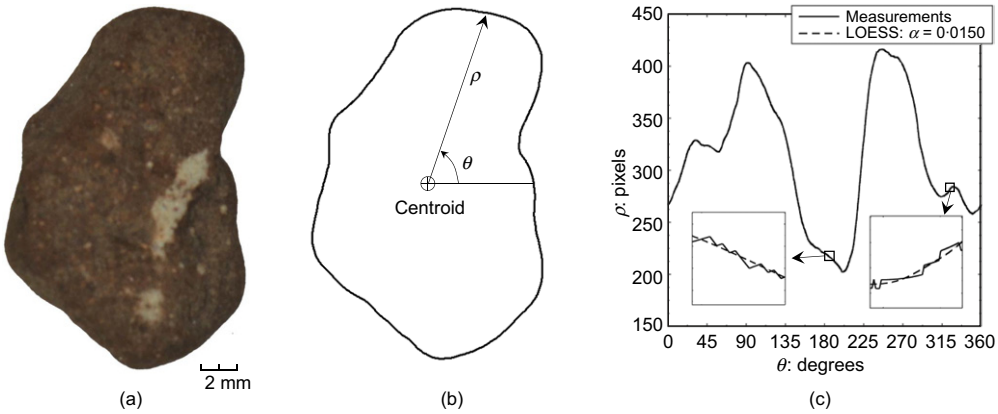

Fig. 7. Particle perimeter profile and roughness assessment: (a) original particle image; (b) particle outline; (c) roughness smoothing by LOESS

ROUNDNESS BY COMPUTATIONAL GEOMETRY

Until now, the computation of roundness has been difficult to automate as it required human judgement. First, the corners on the soil particle had to be identified. Large variations in the number of corners per particle, their curvilinearity and the size of the particles made it difficult to establish a rigorous and repeatable procedure. There are no universal guidelines for identifying corners and for fitting appropriate circles to them. As a result, different human evaluators could find considerably different values for roundness. Second, particle roughness is superimposed over the particle corners. The roughness can be intuitively filtered out by humans when fitting circles to the corners. By contrast, computers have to be taught or programmed to distinguish roughness from small sharp corners. In this section an attempt is made to solve these various challenges.

Removing roughness from particle corners

Previous researchers sought to remove the effects of roughness by discretising the outline of a particle into an N-sided equal-angled polygon. The selected N value would therefore serve as the cut-off between angularity and roughness. Sukumaran & Ashmawy (2001) suggested that $N=40$ would be an appropriate value, while Tutumluer & Pan (2008) believed $N=24$ to be satisfactory. In reality, a single N value cannot be applicable to all soil particles; N should vary from particle to particle depending on the particles' individual angularities and roughnesses. Another limitation of this N approach is that small, sharp corners can easily be missed. As such, it is ineffective for very angular particles. This will be demonstrated by example later in the paper.

The previous section of this paper showed that LOESS and K-fold cross-validation effectively estimate the mean surface. This technique can be used to remove particle roughness. An example soil particle surface was represented using polar coordinates, as shown in Fig. 7. After finding the mean surface, (θ, ρ) could be plotted to show the new 'smoothed' soil particle outline as in Fig. 8. Having the smoothed particle outline, the next step towards computing Wadell's roundness is to fit an appropriate circle to each corner.

Corner identification

Determination of Wadell's roundness requires identification of each particle corner and assessment of its sharpness. In manual methods, judgement and intuition are used to identify the corners, as is done, for example, by the authors in Fig. 9. By contrast, newer definitions of roundness using Fourier analysis, angularity index and the fractal technique measure curvatures over the entire particle outline instead of just corners. As shown in Fig. 9, the full outline of a particle contains both corner (convex) portions and non-corner (concave and flat portions). An algorithm is now presented to extract only the corner portions.

The smoothed outline of a particle can be discretised by 'key points' connected by line segments. An example is given in Fig. 10 where the curve EF represents the full perimeter of the particle in which the amplitudes are radial distances

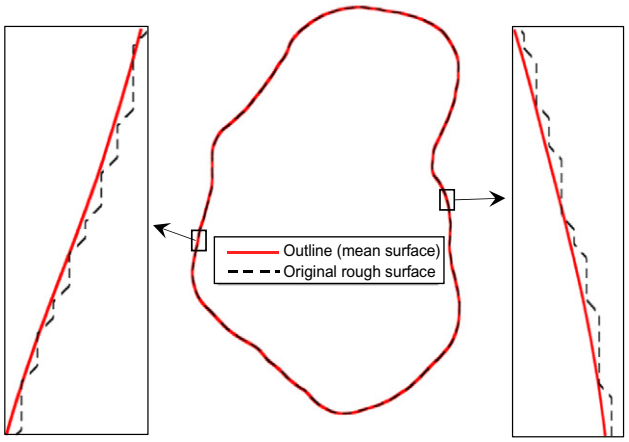

Fig. 8. Removing roughness from the particle outline

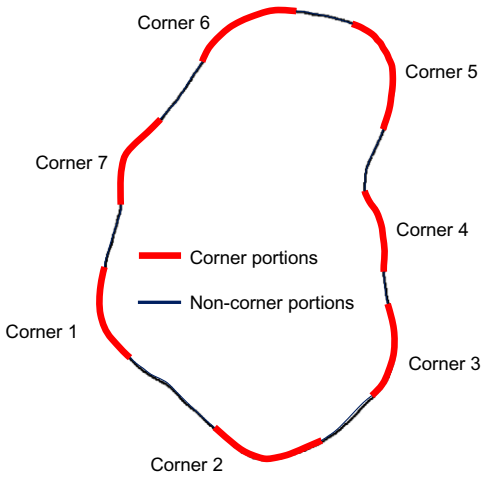

Fig. 9. Corner and non-corner portions of a particle outline

from the particle centroid, as in Fig. 7(c). A line $\overline{EF}$ is first drawn connecting the first and last point of the curve $\widetilde{EF}$ (Fig. 10(a)). Point E is the first point on the discretised curve and F is the last one. The distance from the maximum divergent point G on $\widetilde{EF}$ to $\overline{EF}$ is defined by δ. If δ is larger than a predefined threshold δ_0, point G becomes the new end point of the line and line $\overline{EF}$ is shortened to $\overline{EG}$, as shown in Fig. 10(b). The maximum divergence, δ, between $\widetilde{EG}$ and $\overline{EG}$ is now computed. The iteration continues until a point such as H in Fig. 10(c), is found for which δ is smaller than δ_0. The curved segment $\widetilde{EH}$ is then permanently replaced by the line segment $\overline{EH}$. Point H now becomes the beginning point of the next straight-line segment to be found and $\overline{HF}$ becomes the new starting line segment, as shown in Fig. 10(d). The previously described procedure continues as shown in Fig. 10(e). In the end, the entire originally curved perimeter $\widetilde{EF}$ will have been discretised into small, piecewise, linear segments connecting the key points, as shown in Fig. 10(f).

The smoothed outline of the soil particle shown in Fig. 9 was discretised using the above-described procedure and the result is shown in Fig. 11. The diamond points on the outline are the starting or ending points of the line segments (i.e. the key points). Naturally, the sharper corners having larger curvature require more line segments, whereas flatter portions need fewer key points and line segments. Obviously, the threshold δ_0 is the critical parameter controlling corner identification; its selection will be addressed in detail later.

The next step is to identify the key points as belonging to either corner or non-corner segments. The centroid of the soil particle, O, is selected as the reference point. The present authors use point C and its closest neighbouring points on both sides, A and B, to explain the next step. Straight-line segments OC and AB are constructed as shown. If necessary, the line OC is extended to its intersection with AB at point D. The distances OD and OC are compared. If $OC \leq OD$, then point C is a non-corner point. Conversely, if $OC > OD$ then it is a corner point. This procedure is repeated for every key point on the particle outline. The final result is shown in Fig. 11(b) where corner points are distinguished from non-corner points. Every stretch of consecutive corner points can now be fitted with a circle.

Circle fitting to corners

Gander *et al.* (1994) introduced a method for fitting a circle to a series of data points. The best-fit circle is found by minimising the sum of the squares of the distances between the points and the circle. Using this approach, the appropriate circle for each corner of a particle can be found. An example is shown in Fig. 12. All of the corner points from 1 to 36 are initially used to compute a best-fit circle, as shown in Fig. 12(a). The centre of this circle is C and the radius is R. The minimum distance from C to the particle boundary is computed as T. If T is smaller than R, the fitted circle is not tangential to the particle boundary at T but secant to it. As such, it is not an acceptable circle. If this happens, the end point 36 is eliminated and point 35 becomes the new last point. The points from 1 to 35 are now used to fit a new circle. The recomputed T and R values are compared. If T is still smaller than R, point 35 is eliminated and 34 becomes the new last point. The process continues until a circle is found satisfying $T \approx R$ or if point 3 becomes the last point. Figs 12(b) and 12(c) show that the last point moved from

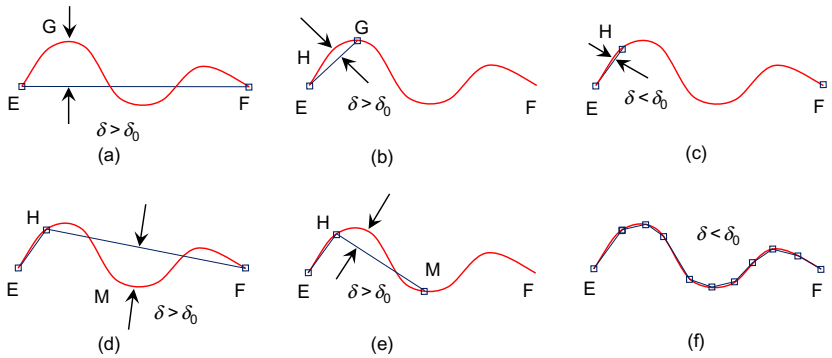

Fig. 10. Discretising the particle boundary

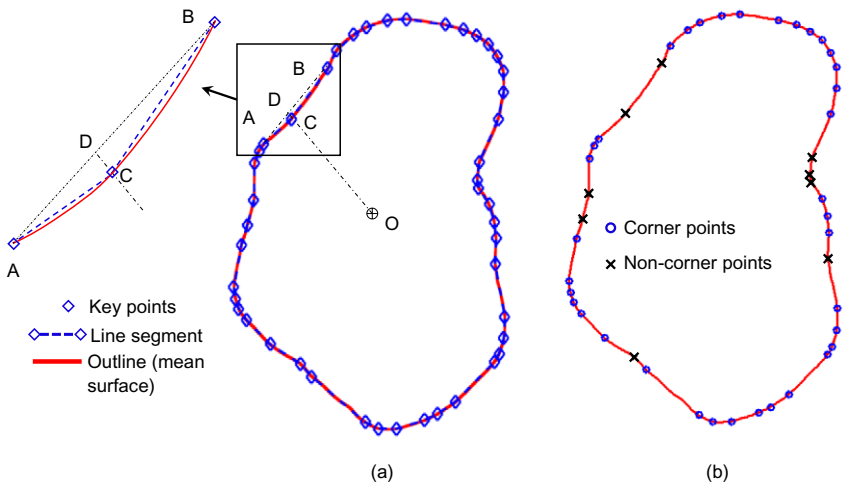

Fig. 11. Identification of particle corners

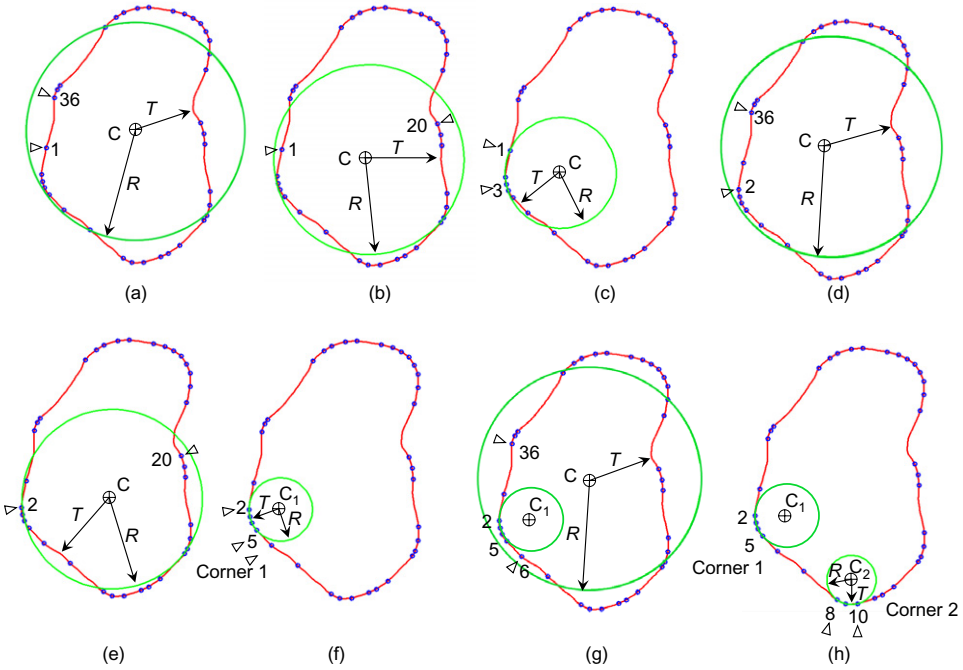

Fig. 12. The circle-to-corner fitting process

point 20 to point 19, then 18, 17, and so on, and all the way to point 3 without finding an acceptable circle. If this happens, the loop ends without an acceptable circle having been found. In the next loop, point 2 becomes the first point, as shown in Fig. 12(d). This time, points 2 to 36 are used to fit a circle and if once again $T < R$ the last point is reassigned to sequentially lower number points in search of a satisfactory circle. Fig. 12(e) shows point 20 as that last point. A proper circle C_1 for which $T = R$ is finally found when point 5 became the last point, as shown in Fig. 12(f). The circle C_1 is the best-fitting circle found using points 2 to 5 for corner 1. The first point now moves to point 6 and point 36 once again becomes the last point in Fig. 12(g). The next satisfactory circle is C_2 fitting points 8 to 10 as shown in Fig. 12(h), which describes the roundness of corner 2. The procedure continues with point 34 finally becoming the first point and point 36 the last.

A special situation must be considered. The first several points (such as points 1 to 3) and the last several points (such as points 34 to 36) may be on the same corner and therefore could be fitted to a same circle in some cases. Therefore, after the last loop, the algorithm needs to check if this may have occurred.

Based on visual observation, the soil particle shown in Fig. 9 appears to have seven corners. For comparison, the results of the 'looping computation' are shown in Fig. 13. Seven circles have been fitted to the corners. The maximum inscribed circle (red circle with centre C_i) is shown in Fig. 13. After determining all the corner circles, the roundness was computed to be 0·49.

In the above procedure, the tangent circle is found by finding the condition where T approximately equals R. However, it is very rare that T is exactly the same as R owing to computational round-off. In fact, the numerous calculations performed for this paper indicate that $0{\cdot}98 \leq T/R \leq 1$ is accurate enough for determining roundness.

ANALYSIS OF δ_0 AND IMAGE RESOLUTION

Discretising the soil particle outline by a sufficient number of key points connected by line segments is essential to identifying the particle corners. A threshold δ_0 must be selected for the discretisation. This δ_0 is the maximum allowed divergence of the curve from the straight line segment approximating it between key points. The chosen value of δ_0 essentially sets the threshold between corners and non-corners. For example, the curve in Fig. 14 will be either identified as a straight line or a corner depending on the chosen value of δ_0. Naturally, δ_0 should be set as small as possible to capture all the corners. However, this would generate more corner points and thus significantly increase the computational effort because the algorithm requires approximately N^N (where N is the number of corner points) operations to find all the corner circles.

Numerous computations were performed to investigate the influence of δ_0 on the final results. They showed that the more angular a soil particle is, the more sensitive the

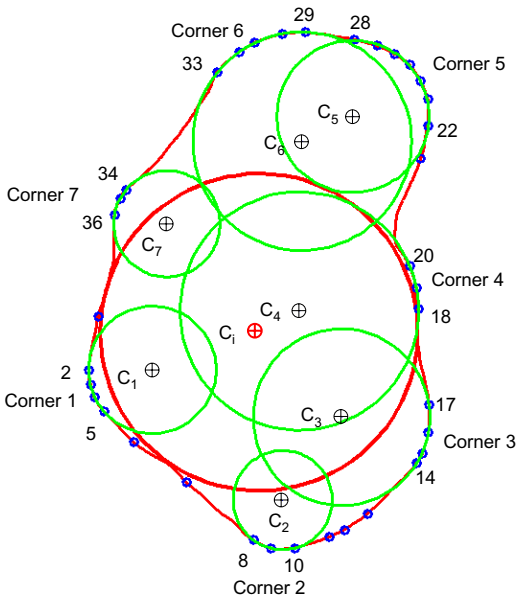

Fig. 13. The final corner fitting of the particle from Figs 11 and 12

roundness results are to δ_0. A very angular soil particle shown in Fig. 15(a) appeared in Powers (1953) and was reported to have a roundness of only 0·12. It has a very complex outline containing many small, sharp corners (e.g. corners 1, 10 and 12) as well as low-curvature corners (e.g. corners 13 and 15).

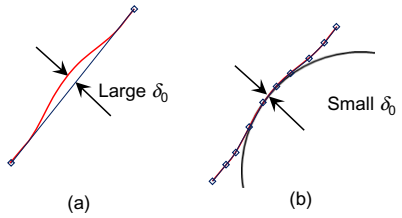

Fig. 14. The definition and significance of δ_0

Thus, it is a particularly challenging particle for the algorithm to compute roundness numerically. As such, it is used here to illustrate the significance of δ_0. A series of δ_0 values was tried and the results are shown in Fig. 15. The original outline of this soil particle contained 3147 points. The δ_0 was first set at 0·01 in Fig. 15(b). In total, 1455 key points including 782 corner points and 673 non-corner points were found. The corner points are plotted on the outline and were fitted by circles. As shown in Fig. 15(b), all 17 corner circles were successfully identified. The computed roundness was 0·12, which agrees perfectly with the value reported by Powers (1953). The δ_0 was then gradually increased from 0·01 to 0·50. Although progressively fewer key points approximated the outline, the computed roundness was exactly the same. However, the computation time was shortened from 2 min for $\delta_0 = 0{\cdot}01$ to less than 1 s for $\delta_0 = 0{\cdot}50$. When δ_0 was further increased to 1·00 (Fig. 15(e)), corners 1, 10, 13

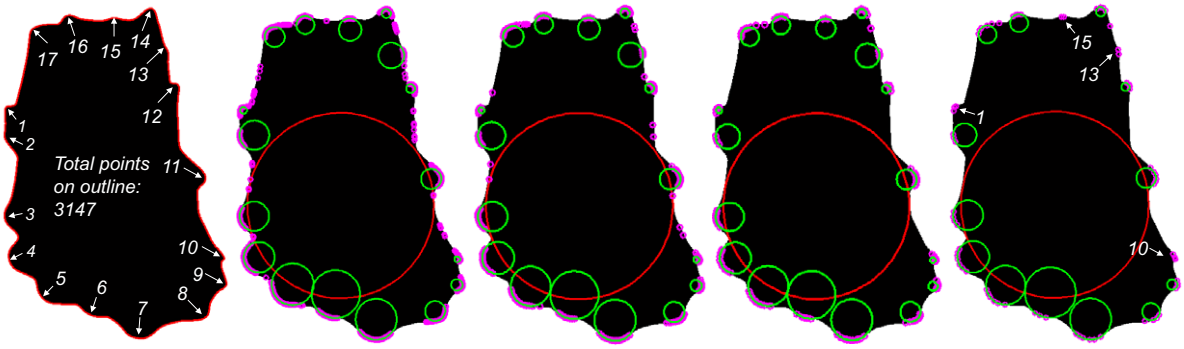

	(a)	(b)	(c)	(d)	(e)
δ_0		0·01	0·1	0·5	1·0
Computed R		0·12	0·12	0·12	0·14
Corner points		782	252	109	72
Non-corner points		673	208	94	60
Computing time		2 min	40 s	<1 s	<1 s

Fig. 15. The effect of different δ_0 values on computed values of roundness

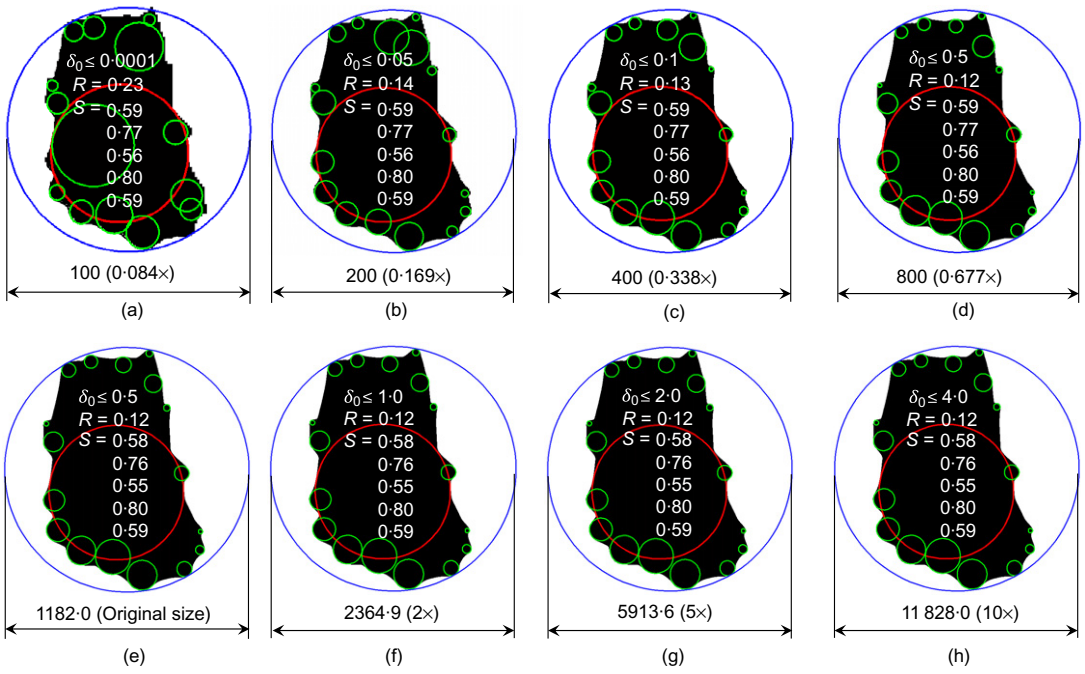

Fig. 16. The influence of PCD on computed values of roundness and sphericity

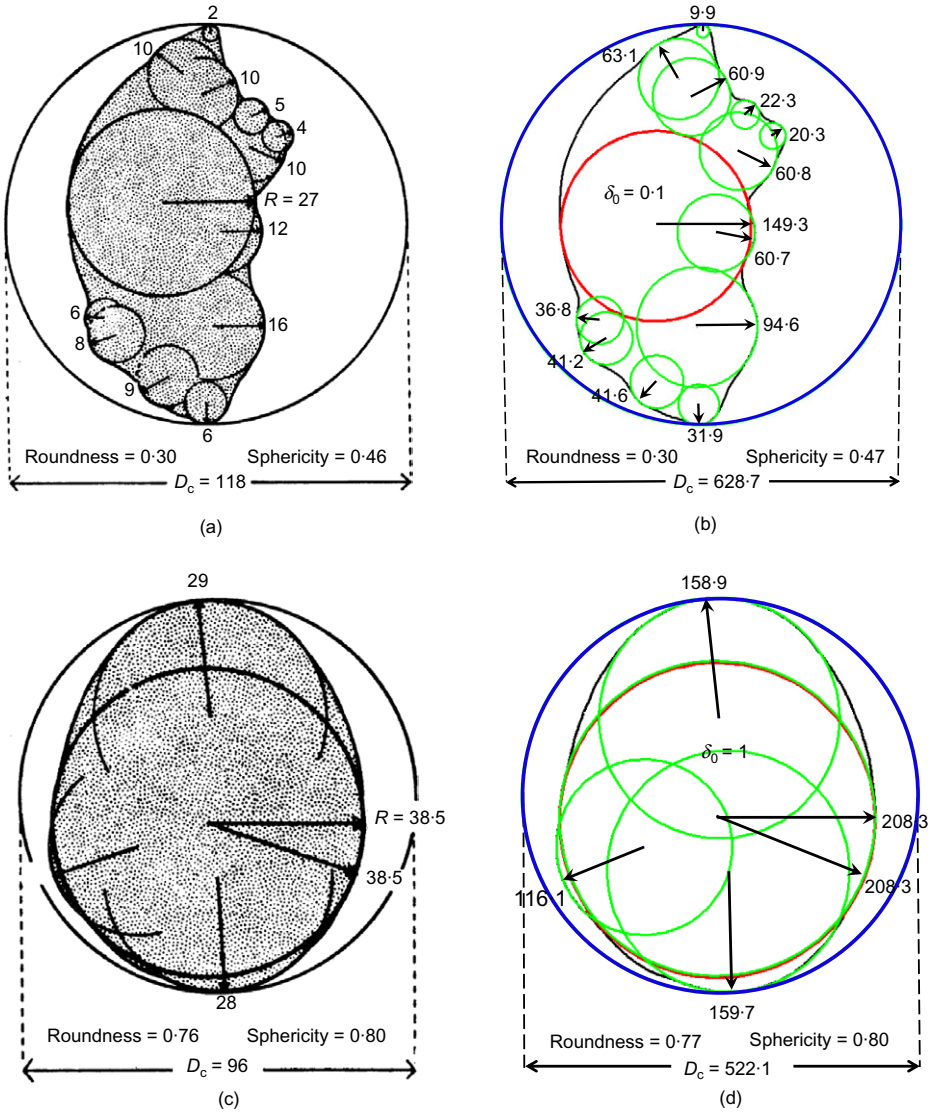

Fig. 17. Comparison to the results of Wadell (1935): (a) and (c) are from Wadell (1935), units are millimetres; (b) and (d) are computational geometry results in pixel units (sphericity is the diameter sphericity by equation (2))

and 15 were not identified and the computed roundness jumped up accordingly. Corners 1 and 10 are very small and sharp whereas corners 13 and 15 have low curvature. These two types of corners are easily missed when using a large δ_0.

It is evident from Fig. 15 that the computed roundness is not very sensitive to δ_0 for values below a specific threshold, $\delta_{0\max}$. When $\delta_0 < \delta_{0\max}$ all of the meaningful particle corners are successfully identified. As such, using values smaller than $\delta_{0\max}$ serves no purpose as it merely decreases computational efficiency. However, the threshold $\delta_{0\max}$ will vary with image resolution (camera magnification). Image resolution is a key factor in the computation of particle roughness, sphericity and roundness. As previously discussed, roughness is a scale-dependent value. For the same surface, different instrument resolutions (e.g. cameras as opposed to microscopes) will yield different roughness values. While there is an obvious dependence of the computed roughness on image resolution, the stability of the computed values of particle sphericity and roundness to different image resolutions is more difficult to assess. To quantify the effect of particle image resolution, the concept of pixels per circumscribed circle diameter (PCD) is introduced. Obviously, the same soil particle will have different PCDs when captured under different camera resolutions.

Compared to rounded particles, the computation of roundness for angular particles is more sensitive to PCD because small, sharp corners may be lost at low PCD. The particle shown in Fig. 15 is again used to demonstrate the influence of PCD on sphericity and roundness. The soil particle was digitally downscaled and upscaled to generate different PCDs as shown in Fig. 16. Sphericity was computed using all five definitions given by equations (1)–(5). Interestingly, the five sphericity values were virtually unaffected when PCD was varied from 100 to almost 12 000. This shows that the sphericity is not sensitive to image resolutions of soil particles for PCD $>$ 100. Roundness values were also computed using the different PCDs and they too are reported in Fig. 16. Several conclusions could be drawn from the results.

(*a*) When PCD is smaller than 200 pixels, significant aliasing was observed along the particle outline. Even when using an extremely small δ_0, the small corners could not be clearly delineated and non-corner parts may have been identified as corners. Therefore, to accurately compute roundness, the particle must be captured with a PCD of at least 200 pixels. Once PCD is larger than 200 pixels, the image resolution is sufficient to delineate even a fairly complex outline.

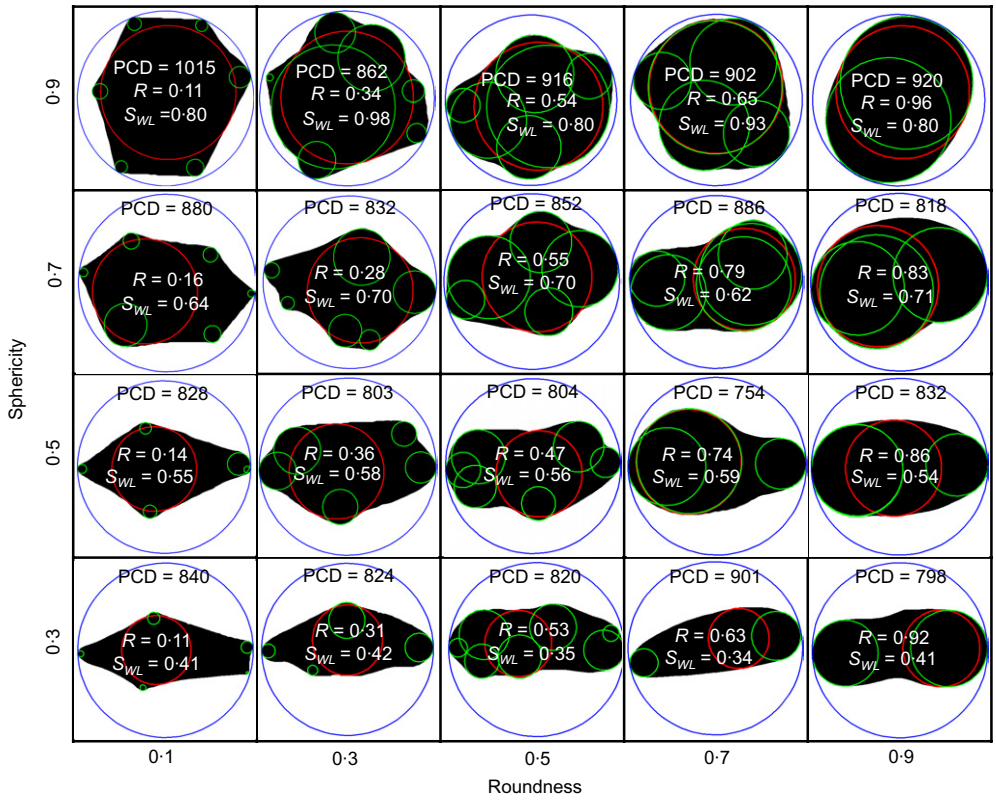

Fig. 18. Comparison of computational geometry results to Krumbein & Sloss (1951)

(*b*) It was shown earlier that, as long as $\delta_0 \leq \delta_{0\max}$, the computed roundness will not be affected. However, the $\delta_{0\max}$ depends on the image resolution, as shown in Fig. 16. The PCD of the soil particle will change under different resolutions. The authors found that $\delta_{0\max}$ should be no larger than 0·03% of PCD.

COMPARISON TO PREVIOUSLY REPORTED SPHERICITY AND ROUNDNESS VALUES

The roundness of the two quartz particles shown in Figs 17(a) and 17(c) were computed manually by Wadell (1935). For comparison, the corner circles were determined using the computational geometry method presented in this paper. The results are shown in Figs 17(b) and 17(d). The positions and sizes of the circles fitted to the corners, as well as the computed roundness values, are very close to those reported by Wadell. Diameter sphericity (equation (2)) which was used by Wadell is also determined by computational geometry. The results again agree with the previously reported values.

Krumbein & Sloss (1951) were first to combine particle sphericity and particle roundness into one chart, as shown in Fig. 18. They evaluated roundness using the method of Wadell (1935), although they did not provide the hand-drawn circles in their published work. The same 20 particles were evaluated for roundness (R) in this paper. The computed maximum inscribed circles and corner circles are shown in Fig. 18. The R values agree well with the values reported by Krumbein and Sloss. Since the proposed computational geometry method appears to yield the same roundness values as by Wadell's manual means or through Krumbein–Sloss chart estimates, the required time, tedium and imprecision of the older methods can now be eliminated.

The method used for computing sphericity by Krumbein & Sloss (1951) is somewhat unclear. They suggested that the

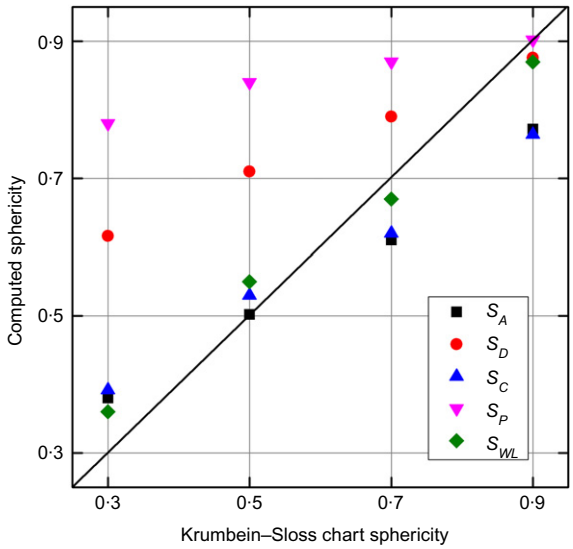

Fig. 19. Comparison of sphericity by various definitions to Krumbein & Sloss (1951) chart values

sphericity values were S_{WL}, which are shown in Fig. 18. However, Santamarina & Cho (2004) and Cho *et al.* (2006) believed the sphericity values in the Krumbein–Sloss charts were S_C. The authors computed sphericity for each soil particle using equations (1)–(5) and compared them with the Krumbein–Sloss chart values in Figure 19. By observation, it appears clear that Krumbein & Sloss (1951) used S_{WL} in their well-known and often-used sphericity chart.

In addition to the widespread historical usage of Fig. 18, there are additional reasons that support the use of the S_{WL} for defining sphericity. First, S_{WL} is conceptually simple, intuitive and easily determined from images. Second,

S_{WL} appears to be completely independent of roundness. Third, of all five definitions, it utilises the largest range of values between 0 and 1·0, thereby making it the most practical and attractive measure of particle form.

CONCLUSIONS

(*a*) This paper has presented methods for determination of soil particle sphericity, roundness and surface roughness using their traditional definitions but obtained numerically through computational geometry. Values for sphericity computed by five existing definitions, all based on two-dimensional particle projections, were compared. The analysis showed that the simple ratio of particle width to length, S_{WL} provides the best distribution of sphericity values between 0 and 1·0 and is also independent of particle roundness.

(*b*) A surface roughness assessment was proposed based on statistical methods: locally weighted regression (LOESS) and *K*-fold cross-validation. A mean surface is determined from which a root-mean-squared roughness is computed. Determination of the mean surface is also a prerequisite to determining particle roundness.

(*c*) The digitisation of Wadell's roundness computation is complex for two reasons. First, the roughness needs to be removed. Second, the particle's corners need to be identified and fitted with appropriate circles. These two challenges were overcome by the computational geometry methods proposed in this paper. The accuracy of the computational algorithm was verified by excellent agreement with original hand computations of roundness. The computational results were also compared to the widely utilised chart of Krumbein & Sloss (1951) to show that the chart's particle silhouettes approximated Wadell's roundness reasonably well. The computational geometry method essentially eliminates the need to use Wadell's manual method and approximations based on the Krumbein–Sloss chart.

(*d*) Parametric evaluation of computational geometry results revealed two rules of thumb for obtaining reliable values of sphericity and roundness. First, the resolution of images should be at least 200 pixels per circumscribing circle diameter (PCD) and, second, the maximum departure of linear segments approximating the particle perimeter ($\delta_{0\max}$) should be no more than 0·03% of PCD.

ACKNOWLEDGEMENTS

This material is based upon work supported by the U.S. National Science Foundation under grant nos. CMMI 0900105 and CMMI 1300010. ConeTec Investigations Ltd and the ConeTec Education Foundation are acknowledged for their support to the Geotechnical Engineering Laboratories at the University of Michigan.

NOTATION

A_s projected area of soil particle
A_{cir} area of minimum circumscribing circle
C_c centre of circumscribing circle
C_i centre of inscribed circle
D_c diameter of circle having the same projected area as the particle
D_{cir} diameter of minimum circumscribing circle
D_{ins} diameter of largest inscribing circle
d_1 length of particle
d_2 width of particle
P_c perimeter of circle having same projected area as the particle
P_s perimeter of particle
R roundness
R_i radius of inscribed circle
S_A area sphericity
S_C circle ratio sphericity
S_D diameter sphericity
S_P perimeter sphericity
S_{WL} width to length ratio sphericity
w_k weight for the kth point in a span
α span distance in LOESS
δ_0 maximum allowed divergence of a curve from the straight line segment approximating it
ε residual error in cross validation
$\hat{\varepsilon}$ average residual error in cross validation
θ, ρ polar coordinates

REFERENCES

Altuhafi, F., O'Sullivan, C. & Cavarretta, I. (2013). Analysis of an image-based method to quantify the size and shape of sand particles. *J. Geotech. Geoenviron. Engng, ASCE* **139**, No. 8, 1290–1307.

Arasan, S., Akbulut, S. & Hasiloglu, A. S. (2011). The relationship between the fractal dimension and shape properties of particles. *KSCE J. Civ. Engng* **15**, No. 7, 1219–1225.

ASTM (2009). *ASTM D 2488-09a: Standard practice for description and identification of soils (visual-manual procedure)*. West Conshohocken, PA, USA: ASTM International.

ASTM (2010). *ASTM D 4791-10: Standard test method for flat particles, elongated particles, or flat and elongated particles in coarse aggregate*. West Conshohocken, PA, USA: ASTM International.

Bareither, C. A., Edil, T. B., Benson, C. H. & Mickelson, D. M. (2008). Geological and physical factors affecting the friction angle of compacted sands. *J. Geotech. Geoenviron. Engng, ASCE* **134**, No. 10, 1476–1489.

Barrett, P. J. (1980). The shape of rock particles: a critical review. *Sedimentology* **27**, No. 3, 291–303.

Bowman, E. T., Soga, K. & Drummond, W. (2001). Particle shape characterization using Fourier descriptor analysis. *Géotechnique* **51**, No. 6, 545–554, http://dx.doi.org/10.1680/geot.2001.51.6.545.

Cabalar, A. F., Dulundu, K. & Tuncay, K. (2013). Strength of various sands in triaxial and cyclic direct shear tests. *Engng Geol.* **156**, No. 1, 92–102.

Chapuis, R. P. (2012). Estimating the in situ porosity of sandy soils sampled in boreholes. *Engng Geol.* 141–142, No. 19, 57–64.

Cho, G.-C., Dodds, J. & Santamarina, C. (2006). Particle shape effects on packing density, stiffness, and strength: natural and crushed sands. *J. Geotech. Geoenviron. Engng, ASCE* **132**, No. 5, 591–602.

Cleveland, W. S. & Devlin, S. J. (1988). Locally weighted regression: an approach to regression analysis by local fitting. *J. Am. Statist. Assoc.* **83**, No. 403, 596–610.

Cox, E. A. (1927). A method of assigning numerical and percentage values to the degree of roundness of sand grains. *J. Paleontol*. **1**, No. 3, 179–183.

Edil, T. B., Krizek, R. J. & Zelasko, J. S. (1975). Effect of grain characteristics on packing of sands. *Proceedings of the Istanbul conference on soil mechanics and foundation engineering*, Istanbul, pp. 46–54.

Efron, B. & Tibshirani, R. J. (1993). *An introduction to the bootstrap*. New York, USA: Chapman and Hall/CRC.

Eisma, D. (1965). Eolian sorting and roundness of beach and dune sands. *Netherlands J. Sea Res.* **2**, No. 4, 541–555.

Ferellec, J. & McDowell, G. (2010). Modelling realistic shape and particle inertia in DEM. *Géotechnique* **60**, No. 3, 227–232, http://dx.doi.org/10.1680/geot.9.T.015.

Frossard, E. (1979). Effect of sand grain shape on the interparticle friction; indirect measurements by Rowe's stress dilatancy theory. *Géotechnique* **29**, No. 3, 341–350, http://dx.doi.org/10.1680/geot.1979.29.3.341.

Galindo-Torres, S. A. & Pedroso, D. M. (2010). Molecular dynamics simulations of complex-shaped particles using Voronoi-based spheropolyhedra. *Phys. Rev. E* **81**, No. 6, 061303.

Galindo-Torres, S. A. & Muñoz, J. D. (2010). Minkowski–Voronoi diagrams as a method to generate random packings of

spheropolygons for the simulation of soils. *Phys. Rev. E* **82**, No. 5, 056713.
Gander, W., Golub, G. H. & Strebel, R. (1994). Least-squares fitting of circles and ellipses. *BIT Numer. Math.* **34**, No. 4, 558–578.
ISO (2008). *ISO 9276-6:2008: Representation of results of particle size analysis – Part 6: Descriptive and quantitative representation of particle shape and morphology*. Geneva, Switzerland: ISO.
Kandasami, R. K. & Murthy, T. G. (2014). Effect of particle shape on the mechanical response of a granular ensemble. In *Geomechanics from micro to macro* (eds K. Soga, K. Kumar, G. Biscontin and M. Kuo), pp. 1093–1098. London, UK: CRC Press.
Katagiri, J., Matsushima, T. & Yamada, Y. (2010). Simple shear simulation of 3D irregularly-shaped particles by image-based DEM. *Granular Matter* **12**, No. 5, 491–497.
Krumbein, W. C. (1941). Measurement and geological significance of shape and roundness of sedimentary particles. *J. Sedimentary Petrol.* **11**, No. 2, 64–72.
Krumbein, W. C. & Sloss, L. L. (1951). *Stratigraphy and sedimentation*. San Francisco, USA: W. H. Freeman and Company.
Kuo, C.-Y. & Freeman, R. B. (2000). Imaging indices for quantification of shape, angularity and surface texture of aggregates. *Transportation Res. Rec*. **1721**, 57–65.
Majumdar, A. & Bhushan, B. (1990). Role of fractal geometry in roughness characterization and contact mechanics of surfaces. *J. Tribol.* **112**, No. 2, 205–216.
Masad, E., Al-Rousan, T., Button, J., Little, D. & Tutumluer, E. (2007). *Test methods for characterizing aggregate shape texture, and angularity*, National Cooperative Highway Research Program Report 555. Washington, D.C., USA: Transportation Research Board.
MathWorks (2014). *MATLAB image processing toolbox*. See http://www.mathworks.com/products/image. (accessed 23/09/2014).
Mehring, J. L. & McBride, E. F. (2007). Origin of modern quartzarenite beach sands in a temperate climate, Florida and Alabama, USA. *Sedimentary Geol.* **201**, No. 2007, 432–445.
Mitchell, J. K. & Soga, K. (2005). *Fundamentals of soil behavior*, 3rd edn,. New York, USA: Wiley.
Mollon, G. & Zhao, J. D. (2012a). Fourier–Voronoi-based generation of realistic samples for discrete modelling of granular materials. *Granular Matter* **14**, No. 5, 621–638.
Mollon, G. & Zhao, J. D. (2012b). Generating realistic 3D sand particles using Fourier descriptors. *Granular Matter* **15**, No. 1, 95–108.
Mollon, G. & Zhao, J. D. (2014). 3D generation of realistic granular samples based on random fields theory and Fourier shape descriptors. *Comput. Methods Appl. Mech. Engng* **279**, 46–65.
Moroto, N. & Ishii, T. (1990). Shear strength of uni-sized gravels under triaxial compression. *Soils Found.* **30**, No. 2, 23–32.
Oh, T. M., Joo, G. W., Yun, K. J. & Cho, G. C. (2014). Crush characteristics of abrasive particles during abrasive waterjet rock cutting. *Proceedings of international symposium on geomechanics from micro to macro*, pp. 1577–1581. London, UK: Taylor & Francis Group.
Powers, M. C. (1953). A new roundness scale for sedimentary particles. *J. Sedimentary Petrol.* **23**, No. 2, 117–119.
Riley, N. A. (1941). Projection sphericity. *J. Sedimentary Petrol.* **11**, No. 2, 94–97.
Rodriguez, J. M., Johansson, J. M. A. & Edeskar, T. (2012). Particle shape determination by two-dimensional image analysis in geotechnical engineering. *Proceedings of Nordic conference on soil mechanics and geotechnics* pp. 207–218. Copenhagen, Denmark: Danish Geotechnical Society.
Rouse, P. C., Fannin, R. J. & Shuttle, D. A. (2008). Influence of roundness on the void ratio and strength of uniform sand. *Géotechnique* **58**, No. 3, 227–231, http://dx.doi.org/10.1680/geot.2008.58.3.227.
Sagga, A. M. S. (1993). Roundness of sand grains of longitudinal dunes in Saudi Arabia. *Sedimentary Geol.* **87**, No. 1993, 63–68.
Santamarina, J. C. & Cho, G. C. (2004). Soil behaviour: the role of particle shape. In *Advances in geotechnical engineering: The Skempton conference*, pp. 604–617. London, UK: Thomas Telford.
Shin, H. & Santamarina, J. C. (2013). The role of particle angularity on the mechanical behavior of granular mixtures. *J. Geotech. Geoenviron. Engng, ASCE* **139**, No. 2, 353–355.
Sladen, J. A., D'Hollander, R. D. & Krahn, J. (1985). The liquefaction of sands, a collapse surface approach. *Can. Geotech. J.* **22**, No. 4, 564–578.
Sukumaran, B. & Ashmawy, A. K. (2001). Quantitative characterization of the geometry of discrete particles. *Géotechnique* **51**, No. 7, 171–179, http://dx.doi.org/10.1680/geot.2001.51.7.619.
Tickell, F. G. (1931). *The examination of fragmental rocks*. Stanford, California, USA: Stanford University Press.
Tutumluer, E. & Pan, T. (2008). Aggregate morphology affecting strength and permanent deformation behavior of unbound aggregate materials. *J. Mater. Civ. Engng* **20**, No. 9, 617–627.
Vepraskas, M. J. & Cassel, D. K. (1987). Sphericity and roundness of sand in coastal plain soils and relationships with soil physical properties. *Soil Sci. Soc. Am. J.* **51**, No. 5, 1108–1112.
Wadell, H. (1932). Volume, shape and roundness of rock particles. *J. Geol.* **40**, No. 5, 443–451.
Wadell, H. (1933). Sphericity and roundness of rock particles. *J. Geol.* **41**, No. 3, 310–331.
Wadell, H. (1935). Volume, shape, and roundness of quartz particles. *J. Geol.* **43**, No. 3, 250–280.
Wang, L., Wang, X., Mohammad, L. & Abadie, C. (2005). A unified method to quantify aggregate shape angularity and texture using Fourier analysis. *J. Mater. Civ. Engng* **17**, No. 5, 498–504.
Wettimuny, R. & Penumadu, D. (2004). Application of Fourier analysis to digital imaging for particle shape analysis. *J. Comput. Civ. Engng* **18**, No. 1, 2–9.
Youd, T. L. (1973). Factors controlling maximum and minimum densities of sands. In *Evaluation of relative density and its role in geotechnical projects involving cohesionless soils* (eds E. T. Selig and R. S. Ladd), STP 523, pp. 98–112. Philadelphia, PA, USA: ASTM International.